Visible Light Communication system using an organic emitter and a perovskite photodetector

Eduardo López-Fraguas[a], Belén Arredondo[b], César Vega-Colado[a], Gonzalo del Pozo[b], Mehrdad Najafi[c], Diego Martín-Martín[b], Yulia Galagan[c], José M. Sánchez-Pena[a], Ricardo Vergaz[a], Beatriz Romero[b]

[a]Electronic Technology Department, Universidad Carlos III de Madrid (GDAF-UC3M), Leganés,28911 Madrid, Spain

[b]Electronic Technology Area, Universidad Rey Juan Carlos (DELFO-URJC), Móstoles, 28933 Madrid, Spain

[c]TNO – Solliance, High Tech Campus 21, Eindhoven 5656AE, The Netherlands

Abstract

The past few years have seen a great increase in the development of Visible Light Communication systems (VLC), mainly triggered by the wide variety of situations they can be used in. These communication systems have traditionally employed inorganic light emitters and photodetectors. In this work, we present a VLC system using an organic emitter and a perovskite photodetector, both fabricated using low cost processing techniques. Perovskite devices have been widely studied as photovoltaics cells since they have achieved great efficiencies, and, in the recent years, there is also an intense research of these devices as photodetectors. In this work, we have fabricated and characterized a perovskite photodetector with layer structure ITO/PTAA/Perovskite/PCBM/BCP/Cu, and integrated it in a visible communication system to successfully link an audio signal.

Keywords: Visible Light Communication, Perovskite Photodetector, OLED.

1. Introduction

The use of light between 400 THz (780 nm) and 800 THz (375 nm) to transmit data has become very popular in the last decades. The main advantages of this spectrum are: i) it is 10,000 times more plentiful than radio frequencies, ii) it does not interfere with WiFi or RF networks, iii) it presents no health risk for humans and iv) its cost and power consumption are low compared to RF[1–5]. In Visible Light Communication (VLC) Systems, data are transmitted by modulating light from an illumination source, such as an ordinary lamp or a LED. Compared to other existing wireless technologies (WiFi, Bluetooth, IrDa, etc.), VLC provides very high data density and very high speed (> 10 Gbps in a few meters indoor system) [6]. The main drawback of this technology is that emitter and receiver have to be in Line of Sight (LOS). VLC applications include water communication [7], inside airplane communication [8], vehicle/road to vehicle [9], indoor broadcast system for internet [10], etc.

VLC photodetectors are usually based on Si or III-V compound materials (mainly InGaAs and GaN), since these are very mature technologies that offer high reliability and high modulation bandwidth (> 1 Gbps) [11]. These technologies, however, need expensive high-temperature and high-vacuum manufacturing processes. With the boost of organic electronics, new VLC systems based on solution-processed organic devices have been developed [12–14]. This technology has several advantages, such as low-cost and scalable fabrication techniques. Besides, organic devices are lightweight, thin, and flexible, very interesting properties for wearable and/or low-cost systems. Using this technology an audio signal has been transmitted with an all-organic flexible VLC prototype [15].

On the other hand, in the last decade a new promising technology has emerged in the field of photovoltaics: perovskite (PVSK) solar cells [16]. This technology has experienced the largest efficiency increase known for any other kind of material in only a few years of development, from 3.8% in 2009 up to 24.2% in 2019 [17]. PVSK devices include a perovskite structured compound, usually a hybrid organic-inorganic lead or tin halide-based semiconductor as the active layer. The most used perovskite structured materials are Methylammonium lead iodide ($CH_3NH_3PbI_3$, MAPI) and Formamidinium lead iodide ($HC(NH_2)2PbI_3$, FAPI), or mixed cations and mixed anions compositions, e.g. Cesium Formamidinium lead halide $Cs_xFA_{1-x}PbI_yBr_{3-y}$. The incorporation of more cations and/or halides has shown to improve the hysteresis and the air stability of the devices [18–20]. Perovskite material is cheap and easy to produce, has tuneable band-gap and large absorption coefficient, ambipolar charge transport, fast response and low-cost fabrication technology. Although perovskites are sensitive to water, UV light and thermal stress, acceptable long-term device stabilities (> 10.000h) have been recently demonstrated by convenient device encapsulation, compositional/interface engineering and the addition of moisture-blocking layers[21,22].

Several authors have already developed and characterized perovskite-based devices as photodetectors, that can ultimately be used in communication systems or imaging applications. In [23] the authors developed all-inorganic perovskite nanostructured photodetectors with high responsivity (>10^6 A/W), high detectivity (>10^{13} Jones) and high device lifetime (2400 h). The authors in [24] demonstrated all-inorganic cesium lead halide perovskite-based photodetectors with high sensitivity (21.5 pW/cm^2), fast response (20 ns) and long stability (2000 h). In [25] the authors showed high performance photodetectors based on organic-inorganic hybrid $CH_3NH_3PbI_{3-x}Cl_x$ using inverted configuration, showing a 3 MHz modulation bandwidth and a detectivity of 10^{14} Jones.

Low-noise (1-2 fA/Hz$^{1/2}$) and high-bandwidth (4.4-1.5 MHz) photodetectors, based on MAPBr and MAPI respectively, have also been developed in [26]. Finally, flexible MAPI based photodetectors with responsivities between 3.5 and 0.0367 A/W at 365 nm and 780 nm respectively have also been demonstrated [27]. In [28] an extensive review of perovskite materials and detectors can be found. Recently, a prototype of a VLC system based on perovskite-based photodetectors and a cool-white commercial LED has been proposed [29]. Authors evaluate three photodetectors based on different active layers, using from single- to triple-cation perovskites. The best performance is achieved with triple-cation perovskites, reaching a bandwidth of around 800 kHz.

In this work we show a VLC system using, for the first time, a hybrid organic-inorganic perovskite photodetector as a receptor and an OLED panel as light source. The layer structure of the photodetector is ITO/PTAA/Perovskite/PCBM/BCP/Cu. Although the layer thicknesses and the device active area were chosen to optimize its performance and stability as a photovoltaic cell, we will show that its performance used as photodetector is comparable to the values found in the literature, being its responsivity, detectivity and bandwidth in the same orders of magnitude of the optimized photodetectors presented previously.

Finally, the VLC system has been validated indoors, transmitting and receiving a good quality audio signal.

2. Experimental methods

Materials and Reagents: All solvents and reagents were of analytically pure quality and used as received. PbI_2 (99.999%) was purchased from TCI. FAI (99.9%), MAI (99.9%), and MABr (99.9%) were purchased from Great Solar. $PbBr_2$ (99.9%), CsI (99.99%), nickel nitrate hexahydrate (98%), dimethylformamide (DMF), dimethylsulfoxide

(DMSO), Bathocuproine (BCP) and PTAA (99.99%) were all purchased from Sigma Aldrich.

Perovskite Device Fabrication: Patterned glass/ITO substrates were ultrasonically cleaned with soap water, deionized water, and ethanol, followed by UV–ozone treatment for 30 min. All the processes were carried out inside the nitrogen-filled glovebox with oxygen and moisture levels 1 ppm. 2mg/ml PTAA was dissolved in chlorobenzene, and solution spin-coated on glass/ITO substrate at 5500 rpm for 30 s. Then samples are annealed on a hotplate at 100 °C for 10 min in a nitrogen-filled glove box. The details of perovskite solution preparation were mentioned in our previous works [30,31]. Briefly, dual cation perovskite $Cs_xFA_{1-x}Pb(I_{1-y}Br_y)$ precursor solutions were deposited from a precursor solution containing FAI, PbI_2, CsI and $PbBr_2$ in anhydrous DMF:DMSO (vol. ratio = 9:1). The perovskite solutions were spin coated in a two-steps program at 2000 rpm for 10 seconds and 5000 rpm for another 30 seconds. During the second step, 300 μL of chlorobenzene was poured on the spinning substrate 20 s prior to the end of the program. The perovskite films were further annealed on a hotplate at 100 °C for 10 min in a nitrogen-filled glove box. After the perovskite film cooled down to room temperature, a 20 mg mL^{-1} PCBM solution in chlorobenzene was spun cast onto the perovskite layer at 1500 rpm for 50 s. Then 1 mg mL^{-1} BCP in chlorobenzene solution was deposited onto the PCBM layer at 4000 rpm for 30 s. Finally, the samples were completed by thermally evaporating 100 nm of Cu under the pressure of 1×10^{-6} mbar through a shadow mask on top of the electron transport layers. Figure 1 shows the layer structure of the perovskite photodetector.

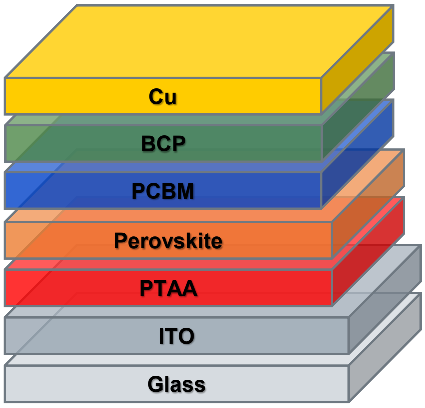

Figure 1. Device layer structure

Characterization methods: The EQE was measured using a lock-in amplifier, a GaSb-detector, a halogen tungsten lamp and a mechanical chopper. J-V curves were measured using a FAS-2 Gamry potentiostat-galvanostat, performing a cyclic voltammetry experiment in order to detect the possible hysteresis of the device, with a 1mV step at a 25 mV/s scan rate, from -0.5 V to 1.3 V. To retrieve the spectral responsivity, we have measured J-V curves while illuminating with Sunbox. This is a proprietary AAA-class solar simulator developed at GDAF-UC3M and described in [32], for devices with sizes similar to our PVSK-PD. We applied different light intensities using a linear current sweep, driving LEDs emitting at 451 nm, 540 nm and 650 nm central wavelengths, and registering the J-V curve at each wavelength.

Impedance measurements were registered with a Solartron 1260 impedance analyser, using a 20 mV sinusoidal signal with a frequency sweep from 1 MHz to 0.1 Hz. The bandwidth measurements were performed modulating a standard green LED using a high-sensitivity HF2LI lock-in amplifier from Zurich Instruments (Zurich, Switzerland). This was combined with a HF2TA transimpedance current amplifier with a gain of 10kV/A and an equivalent input impedance of 50 Ω, in order to transduce the 0 V-biased PVSK-PD current generated by the incoming light from the modulated LED, and connected to the lock-in amplifier to get a simultaneous measurement of excitation and response.

3. Results and discussion

In this section, we present the opto-electrical characterization of the perovskite photodetector and show that the device meets the requirements in terms of responsivity, detectivity and modulation response in order to be integrated in a VLC system. The characterization of the flexible organic light emitting panel used as luminaire is described in a previous work [15]. Finally, we describe the performance of the VLC system, emphasizing that this perovskite photodetector allows a robust optical link for real audio data transmission.

3.1 Perovskite Photodetector Characterization

External quantum efficiency (EQE) is an important figure of merit for optical detectors and photovoltaic devices. It is defined as the ratio between the photogenerated electrons extracted from the device over the incident photons, as a function of wavelength. Our devices exhibit an EQE at zero bias of around 80% in a broad-spectrum range, from 380 nm up to 800 nm, covering the visible spectra and entering the near infrared (see Figure 2). The EQE maximum is 0.86 at 630 nm, indicating that the device active layer thickness is optimized to reach an optimal trade-off between minority carrier generation and recombination. The active layer is thick enough to exhibit a good absorption, and further increasing of the thickness would increase series resistance and bulk recombination, therefore with no significant improvement of light harvesting. On the contrary, thinner perovskite layers present a very low shunt resistance, consistent with a substantial increase in recombination at the grain boundaries and interfaces [33]. Moreover, the EQE exhibits a flat behaviour in the visible interval of the spectrum, making it suitable for VLC applications.

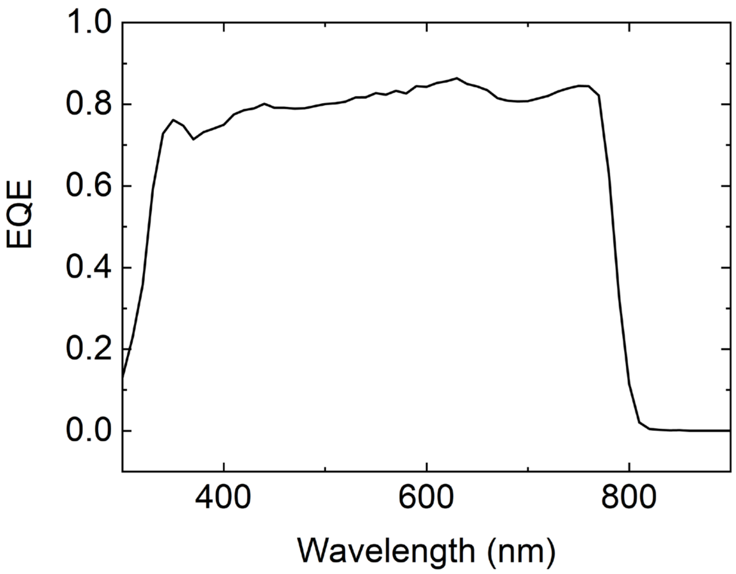

Figure 2. EQE of the PVSK photodetector.

Figure 3a shows the measurements that allow the retrieval of the experimental responsivity at 451 nm, 540 nm and 650 nm. Responsivity was obtained by increasing the optical intensity at every wavelength and measuring the short-circuit current in each case.

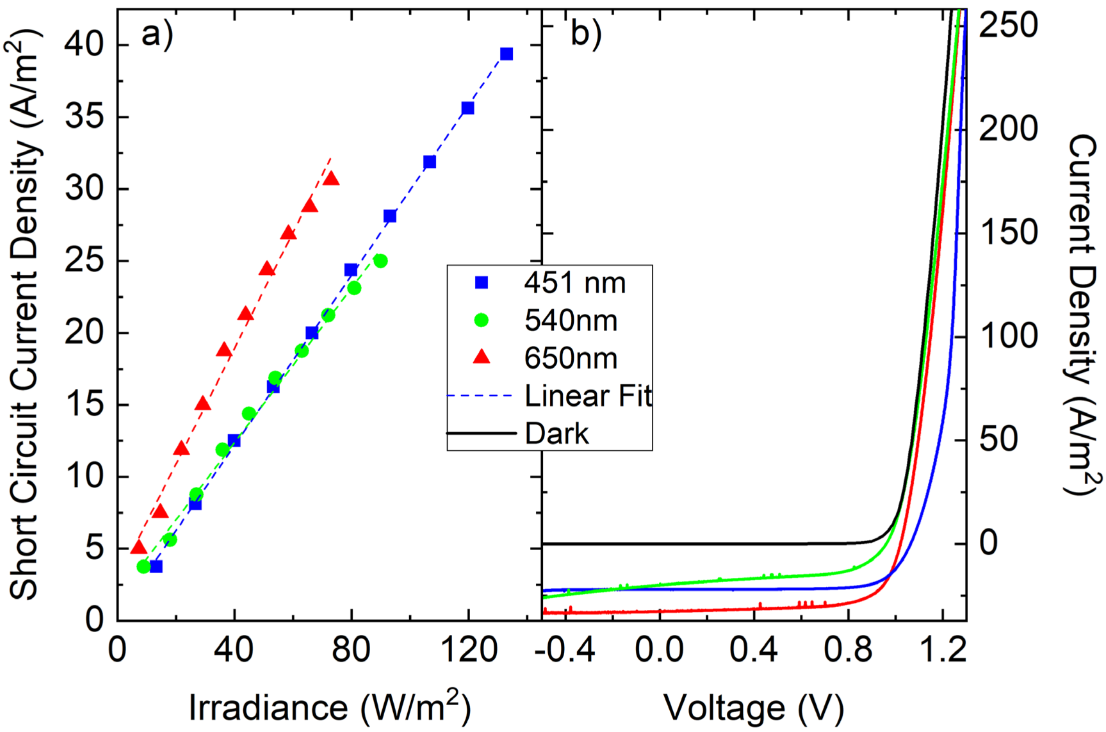

Figure 3. a) Short circuit current vs incident irradiance at 451, 540 and 650 nm for different light intensities, b) J-V curve in dark and under 73 W/m^2 illumination.

The responsivity is obtained from the slope of the linear fit of current J vs light intensity Φ,

$$\left.\frac{\partial J}{\partial \Phi}\right|_{451nm} = 0.296\left[\frac{A}{W}\right]$$
$$\left.\frac{\partial J}{\partial \Phi}\right|_{540nm} = 0.269\left[\frac{A}{W}\right] \qquad (1)$$
$$\left.\frac{\partial J}{\partial \Phi}\right|_{650nm} = 0.403\left[\frac{A}{W}\right]$$

The spectral responsivity SR relates theoretically to the EQE using Eq 2, ,

$$SR\left[\frac{A}{W}\right] = \frac{q\lambda}{hc} * EQE\left[\frac{e^-}{ph}\right] \qquad (2)$$

Where q is the electron charge, λ the incident wavelength, h the Planck's constant and c the speed of light. Using the previous equation and the obtained responsivity we retrieve the theoretical EQE at these wavelengths.

$$EQE_{451nm} = \frac{hc}{q\lambda} * SR_{451nm} = 0.814$$
$$EQE_{540nm} = \frac{hc}{q\lambda} * SR_{540nm} = 0.618 \qquad (3)$$
$$EQE_{650nm} = \frac{hc}{q\lambda} * SR_{650nm} = 0.769$$

There is good agreement at 451 nm and 650 nm, however, at 540nm the EQE exhibits a non-negligible deviation (0.618 against around 0.8). This can be attributed to the wide emission spectrum of the LED used to measure the responsivity at that wavelength, far away from being monochromatic (see [32]).

Figure 3b shows the Current Density-Voltage (J-V) characteristic measured in forward scan, both under dark and illuminating with the three colours with a light intensity of 73 W/m^2. Perovskite detectors, as well as solar cells, typically exhibit hysteresis in the J-V curve when measured in forward and reverse potentiostatic scan, and this affects power conversion efficiency dramatically. When measuring these perovskite devices as photodetectors operating at zero bias, the photocurrent remains almost unchanged under the same monochromatic light irradiance for forward scan, and it agrees with the data obtained from the short-circuit current measured in steady state.

The dark current of a photodiode is a source of noise when used in an optical communication system. This PVSK-PD exhibits a dark current density as low as 0.14 nA/cm^2. The specific detectivity (D^*) is another important figure of merit of a photodetector since it indicates the ability to detect low signals, and is given by Eq.4,

$$D^* = \frac{R}{\sqrt{2eJ_{dark}}} \quad (4)$$

Table 1 shows $D*$ and the Noise Equivalent Power (NEP), which is given by $NEP = \sqrt{A}/D*$, being A the device area (0.16 cm^2), for the three wavelengths using the experimental values of responsivity R and dark current J_{dark},

Parameter	451 nm	540 nm	650 nm
NEP ($W/Hz^{1/2}$)	$9x10^{-15}$	$9.9x10^{-15}$	$6.6x10^{-15}$
D* (Jones)	$4.5x10^{13}$	$4.1x10^{13}$	$6.1x10^{13}$

Table 1. Noise equivalent power (NEP) and detectivity at three wavelengths of the PVSK-PD.

In summary, our photodetector exhibits values of R, $D*$ and J_{dark} comparable to similar devices reported in literature [34,35], and it meets the requirements to be used in an audio link.

The modulation bandwidth of the photodetector was measured using a standard green LED driven by a lock-in amplifier, and registering the photogenerated current with a trans-impedance amplifier detailed in the Experimental Section. The bandwidth at -3dB is defined as the frequency of the light signal at which the photocurrent drops to 70.7% of its value under steady illumination conditions. The bandwidth for this PVSK-PD at zero bias is estimated to be around 116 kHz (see Figure 4). It is well known that bandwidth increases with reverse bias for inorganic and organic photodetectors. However, strong reverse bias accelerates degradation processes in perovskite devices [36]. For this reason, authors chose a conservative photodetector bias of zero volts, since it behaves with a similar spectral response and widely covers audio data transmission.

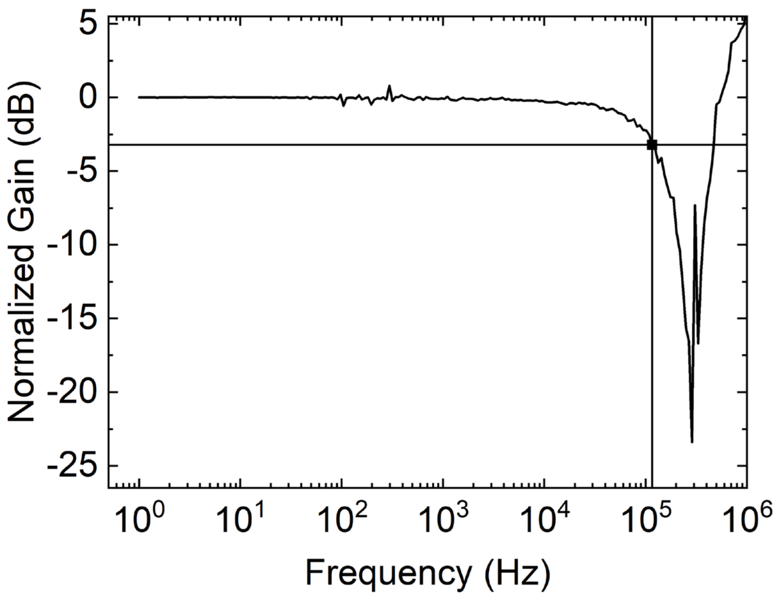

Figure 4. Dynamic modulation response at zero bias

The experimental bandwidth can be verified through the fit of an impedance spectroscopy measurement using an equivalent circuit [37]. Figure 5 shows two representations of the impedance spectra at zero bias: Cole-Cole plot (complex versus real part of the impedance with the frequency as an implicit variable) and Bode diagram. We performed the impedance measurement illuminating with the same green LED used in bandwidth measurement. The inset of Figure 5a clearly shows that there are two semicircles, one at high frequencies (the left one at Cole-Cole plot) that has been previously related to diverse dipolar mechanisms, and another one at lower frequencies associated to ion migration to the electrodes [38]. We obtain the characteristic times of these two features by fitting the impedance spectra with the circuit shown in the inset of Figure 5b. We chose the simplest circuit that most accurately fit the experimental results, obtaining very good fits (solid lines of Figure 5). The circuital model is composed of a series inductance L_s to model the effect of wires at high frequency, a series resistance R_s that accounts for non-ohmic contacts of wires and soldering. The high frequency characteristic is modelled with C_{HF} (geometrical capacitance) and R_{HF} , and the low the frequency behaviour is modelled with

R_{LF} and C_{LF}, being C_{LF} the low frequency capacitance of the *CPE* (Constant Phase Element), a non-ideal capacitor with $Z_{CPE} = 1/(C_{LF})(j\omega)^{CPE_P}$ when the CPE_P value is close to 1. In the DC regime and assuming an ideal infinite shunt resistance, the dynamical diode resistance is R_{HF}+R_{LF}, contributing both R_{HF} and R_{LF} to recombination.

According to Zarazua et al. [39], in perovskite devices, the high frequency elements (C_{HF} and R_{HF}) are related to dielectric and recombination properties. Mechanisms associated to C_{LF} and R_{LF} are still under debate, most authors agree that they are related to slower mechanisms of carrier accumulation and ion migration, which might be responsible of the hysteretic behaviour of I-V curves. Either way, the discussion of the physical mechanisms occurring in perovskite devices is far beyond the scope of this work.

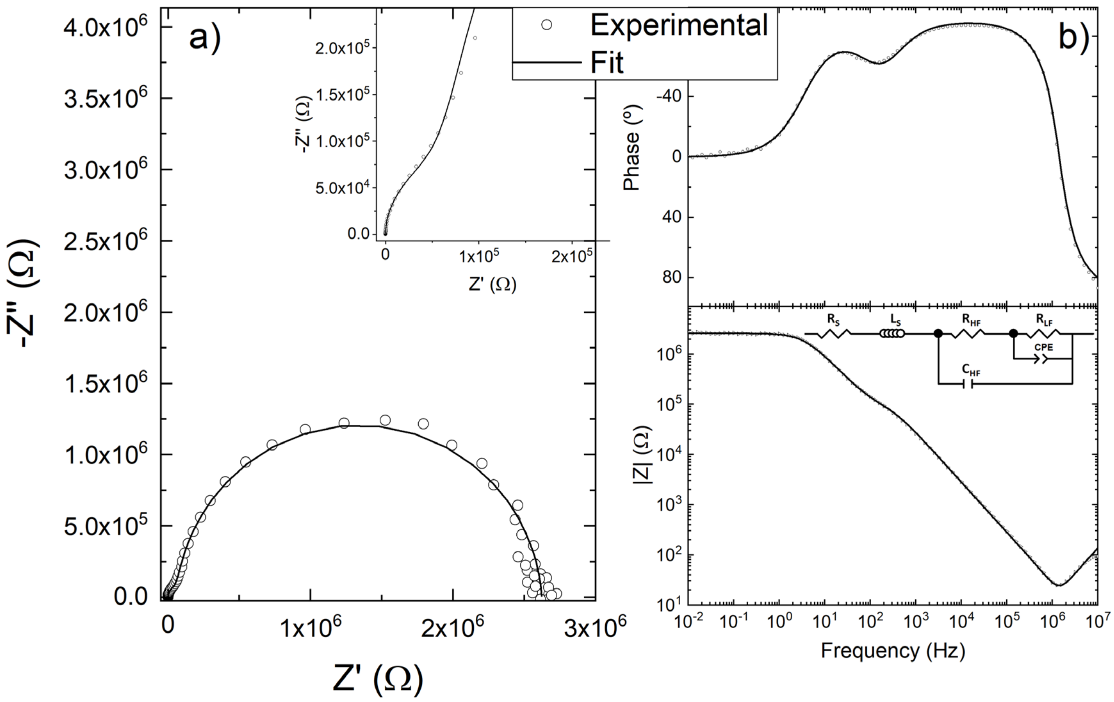

Figure 5. Impedance spectra at zero bias. a) Nyquist diagram, b) Bode diagram. Insets show a zoom of the high frequency range in a) and the small signal circuit to fit the impedance in b).

The circuital parameters obtained from the fit are shown in table 2. All parameters present an error below 5%.

Parameter	Value	Error (%)
Ls (H)	2.22 x10-6	1.28
Rs (Ω)	$2.4x10^{1}$	1.55
R_{LF} (Ω)	$2.47x10^{6}$	0.91
R_{HF} (Ω)	$1.49x10^{5}$	3.4
C_{HF} (F)	$5.67x10^{-9}$	0.65
C_{LF} (F)	$1.47x10^{-8}$	4.74
CPE_P	0.94	1.06

Table 2. Circuital parameters obtained from the fit of Figure 5.

Using the above parameters, we can estimate the -3dB cut-off frequency using the equivalent circuit of the PVSK-PD related to the bandwidth measurement circuit, as shown in Figure 6. We can restrict it to the high frequency effects to obtain the -3dB cut-off frequency.

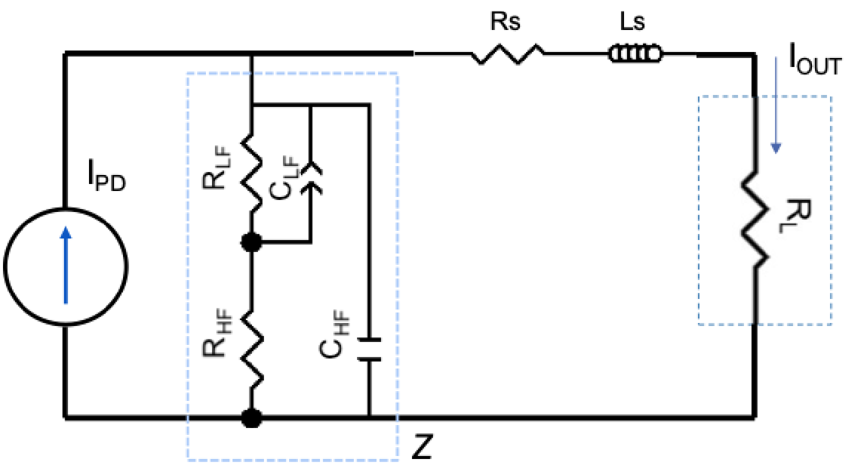

Figure 6. AC equivalent circuit for the OPD in the bandwidth measurement. Illumination with a modulated green LED generates an AC photogenerated current source I_{PD} in the PVSK-PD registered with a trans-impedance amplifier of R_L input impedance.

To that purpose, we consider the following in circuit of Figure 6: i) the current source, I_{PD}, is the small signal part of the photogenerated input current when the green LED modulated light is impinging the perovskite photodetector. ii) the resistance R_L is the trans-impedance amplifier load resistance used to obtain the bandwidth measurements, retrieved from the datasheet. We can neglect the effect at very high frequencies modelled by *Ls*, as they appear over 10^6 Hz, i.e., above the cut-off frequency (see Figure 5b). Eq. 5 describes the transfer function of the circuit,

$$\frac{I_{OUT}}{I_{PD}} = \frac{Z}{Z+Rs+R_L} \quad (5)$$

It is also possible to neglect the effect of R_{LF} and C_{LF}, since these parameters model the medium-low frequency part of the spectra and we are focusing on higher frequencies. Thus, the current gain at high frequency is given by Eq.6,

$$\frac{I_{OUT}}{I_{PD}} \cong \frac{R_{HF}/(R_S+R_{HF}+R_L)}{1+j\omega\frac{C_{HF}R_{HF}(R_S+R_L)}{R_S+R_{HF}+R_L}} \quad (6)$$

This transfer function exhibits a pole with a corresponding linear frequency given by Eq.7:

$$\frac{1}{2\pi[R_{HF}||(R_S+R_L)]} \quad (7)$$

Using a load resistance for the trans-impedance amplifier of 50 Ω results in a cut-off frequency of 380 kHz. This value is in the same order of magnitude as the measured cut-off frequency, though three times bigger. According the Eq. 7, the cut-off frequency is dominated by Rs, and this resistance is quite dependent on the experimental set-up. A slight increase in the Rs due to wires, soldering, etc, could dramatically decrease the bandwidth measurement. Moreover, transfer function of Eq. 6 is obtained assuming the dominant pole approximation, which may also introduce a slight error in the theoretical frequency.

3.2 VLC system

The VLC system is built around the light link established between a LED luminaire and the above described perovskite-based photodiode (see Figure 7). The VLC system consists of a circuit to drive the luminaire, called the Emitter subsystem, and a circuit to process the signal received at the perovskite photodiode, called the Receiver subsystem. The Emitter subsystem takes the signal coming from an audio source, selected as a proof of concept to validate the system performance. The source can be any other signal, provided that the transmission rate is within the whole system bandwidth.

Once the signal arrives to the Emitter, a simple non-inverting amplifier sends the signal to the next stage. The transmitted signal is frequency modulated using a voltage-controlled oscillator (VCO) as modulator. In this circuit, the frequency of the modulated signal is linearly dependent on the voltage level of the incoming signal. After the VCO, a power stage drives the necessary current to the LED luminaire.

The luminaire in the VLC system must continue working as an illumination system while the information is being transmitted, and no user should be aware of the communication system underneath the lightning. In this way, the power stage must guarantee that the emitted light keeps a constant mean value to serve as a constant illumination source, while the AC signal to be transmitted produces a superimposed variable light that carries the information through its frequency, in an imperceptible way for a human eye.

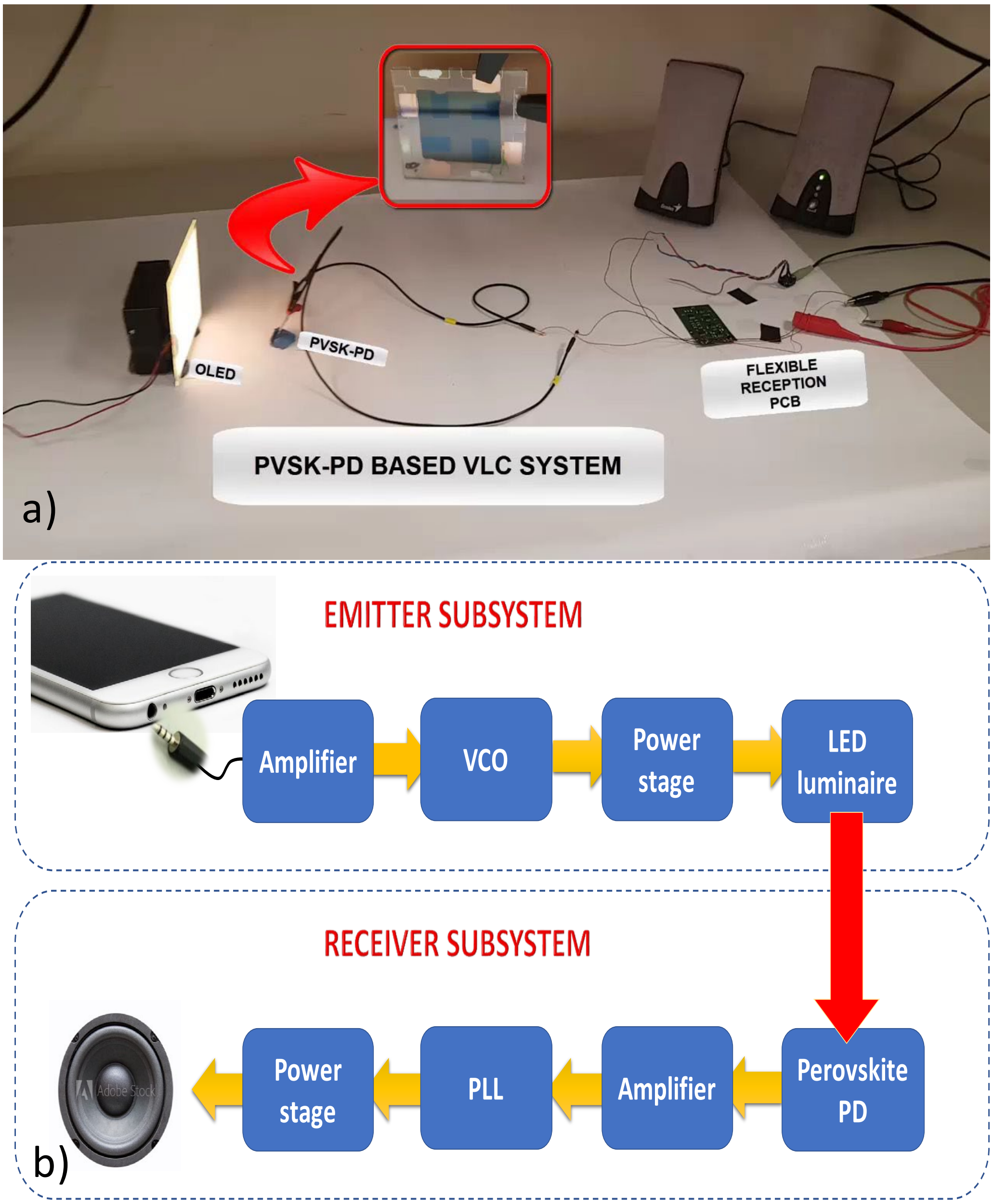

Figure 7: a) Photograph and b) Emitter and receiver subsystems block diagram of the VLC system

The aim of this work is to produce a proof of concept of a modern VLC system using a flexible OLED luminaire 99 × 99 × 0.88 mm LG N6SA30 with a power consumption of 1.28 W. This OLED panel exhibits an efficacy of 60 lm/W and an ease installation, suitable to be used as a spotlight in any application regarding a low-range link, such as those in working environments, communications in car systems, illumination in patients' beds in hospitals or artworks in museums. Its flexibility makes it ideal for communications into different parts of a security force or military suit, towards wearable applications, etc.

The Receiver subsystem uses the perovskite photodiode. It collects the light coming from the luminaire. As we have shown, the speed response of the PVSK-PD is more than sufficient for the frequency range of the transmitted audio signal. A transimpedance amplifier + filter stage separates the DC and AC components of the signal, amplifying the small signal. To track the incoming frequency and to convert it linearly to a voltage level, a phase locked loop (PLL) is inserted as the next stage. This stage demodulates the signal, and the result of this frequency-to-voltage demodulation is a voltage signal that retrieves the information of the transmitted signal. A final power stage provides the necessary current to drive a loudspeaker with the demodulated signal. Biasing the OLED near the forward voltage results in better operation, since it eases the OLED switching without affecting the lighting level, and simultaneously it improves the switching speed of the OLED.

Every component used in the system is an off-the-shelf. Both the VCO and the PLL have been implemented using CD4046 integrated circuits. The audio amplifier uses a standard LM386. The receiver circuit has been mounted on a flexible PCB (Würth Electronics), with the aim of being part of a possible wearable system.

We have tested this whole system using an audio signal. The signal frequency is under 20 kHz. Following Nyquist theorem, we have sent the information using a 44 kHz signal. The retrieved signal at the end of the channel does not show any deviation from the original one. The demonstration video included in the Supplementary information proves that the audio signal is recovered without any significant distortion.

Conclusions

We have reported a prototype VLC system with a perovskite photodetector in the receiver subsystem and a flexible organic white LED in the emitter system that successfully links an audio signal. The layer structure of the perovskite device is ITO/PTAA/Perovskite/PCBM/BCP/Cu. The perovskite photodetector exhibits responsivities of 0.296 A/W, 0.269 A/W and 0.403 A/W at 451 nm, 540 nm and 650 nm respectively. The photodetector dark current is as low as 0.14 nA/cm^2, resulting in detectivities of 4-6x10^{13} Jones for the visible spectra, and indicating a good ability to detect very low signals. The photodetector bandwidth is ~120 kHz, that widely allows audio data rate. Finally, the presented VLC proof of concept is cost effective, since the whole system was designed and built using low cost components.

This work demonstrates the feasibility of using a perovskite photodetector in a VLC system. Moreover, this kind of photodetectors are expected to be more suitable for VLC links in applications involving wearables or any other flexible items, reducing also the fabrication costs and easing their integration. Furthermore, the increasing interest in perovskite materials to be used in solar cells and photodetectors also boost the interest in new applications. Although the measurement bandwidth is around 120 kHz, this data rate is enough for any communication system transmitting audio and text. We think that it should be of special interest in museums guides, hospitals, intra-vehicle communications and technical aids for disabled people, where the amount of information is not as important as the ergonomics, privacy, communication security, economy and quality of the instrumentation used.

Acknowledgements

This work has been supported by Comunidad de Madrid under the SINFOTON2-CM Research Program (S2018/NMT-4326-SINFOTON2-CM), and the Spanish Ministry of Economy, the Agencia Estatal de Investigación and European Union's FEDER under the TEC2016-77242-C3-(1-R and 3-R) AEI/FEDER, UE Projects. The work of E. López-Fraguas was supported by the Ministerio de Educación y Formación Profesional for his Doctoral Grant through FPU Research Fellowship under Grant FPU17/00612. The work of M.N. and Y.G. was supported by Solliance, a partnership of R&D organizations from the Netherlands, Belgium, and Germany working in thin film photovoltaic solar energy. Authors wish to thank Iván García and Ignacio Rey-Stolle from the Polytechnic University of Madrid and Cristina de Dios and Angel R. Criado from LuzWavelabs for their valuable help in the EQE and bandwidth measurements, respectively.

References

[1] T. Komine, M. Nakagawa, Fundamental analysis for visible-light communication system using LED lights, IEEE Trans. Consum. Electron. 50 (2004) 100–107. doi:10.1109/TCE.2004.1277847.

[2] A. Jovicic, J. Li, T. Richardson, Visible light communication: opportunities, challenges and the path to market, IEEE Commun. Mag. 51 (2013) 26–32. doi:10.1109/MCOM.2013.6685754.

[3] D. Tsonev, H. Chun, S. Rajbhandari, J.J.D. McKendry, S. Videv, E. Gu, M. Haji, S. Watson, A.E. Kelly, G. Faulkner, M.D. Dawson, H. Haas, D. O'Brien, A 3-Gb/s Single-LED OFDM-Based Wireless VLC Link Using a Gallium Nitride $\mu\rm LED$, IEEE Photonics Technol. Lett. 26 (2014) 637–640. doi:10.1109/LPT.2013.2297621.

[4] P.H. Pathak, X. Feng, P. Hu, P. Mohapatra, Visible Light Communication, Networking, and Sensing: A Survey, Potential and Challenges, IEEE Commun. Surv. Tutor. 17 (2015) 2047–2077. doi:10.1109/COMST.2015.2476474.

[5] H.L. Minh, D. O'Brien, G. Faulkner, L. Zeng, K. Lee, D. Jung, Y. Oh, E.T. Won, 100-Mb/s NRZ Visible Light Communications Using a Postequalized White

LED, IEEE Photonics Technol. Lett. 21 (2009) 1063–1065. doi:10.1109/LPT.2009.2022413.

[6] Z. Ghassemlooy, L.N. Alves, S. Zvanovec, M.-A. Khalighi, Visible Light Communications: Theory and Applications, CRC Press, 2017.

[7] F. Miramirkhani, M. Uysal, Visible Light Communication Channel Modeling for Underwater Environments With Blocking and Shadowing, IEEE Access. 6 (2018) 1082–1090. doi:10.1109/ACCESS.2017.2777883.

[8] R. Perez-Jimenez, J. Rufo, C. Quintana, J. Rabadan, F.J. Lopez-Hernandez, Visible Light Communication Systems for Passenger In-Flight Data Networking, Ieee, New York, 2011.

[9] T. Yamazato, I. Takai, H. Okada, T. Fujii, T. Yendo, S. Arai, M. Andoh, T. Harada, K. Yasutomi, K. Kagawa, S. Kawahito, Image-sensor-based visible light communication for automotive applications, IEEE Commun. Mag. 52 (2014) 88–97. doi:10.1109/MCOM.2014.6852088.

[10] J. Grubor, S. Randel, K. Langer, J.W. Walewski, Broadband Information Broadcasting Using LED-Based Interior Lighting, J. Light. Technol. 26 (2008) 3883–3892. doi:10.1109/JLT.2008.928525.

[11] L. Grobe, A. Paraskevopoulos, J. Hilt, D. Schulz, F. Lassak, F. Hartlieb, C. Kottke, V. Jungnickel, K. Langer, High-speed visible light communication systems, IEEE Commun. Mag. 51 (2013) 60–66. doi:10.1109/MCOM.2013.6685758.

[12] B. Arredondo, B. Romero, J.M. Sanchez Pena, A. Fernandez-Pacheco, E. Alonso, R. Vergaz, C. de Dios, Visible Light Communication System Using an Organic Bulk Heterojunction Photodetector, Sensors. 13 (2013) 12266–12276. doi:10.3390/s130912266.

[13] H. Chen, S. Li, B. Huang, Z. Xu, W. Li, G. Dong, J. Xie, A 1.9Mbps 01DM-based All-Organic Visible Light Communication System, Ieee, New York, 2016.

[14] P.A. Haigh, Z. Ghassemlooy, S. Rajbhandari, I. Papakonstantinou, Visible light communications using organic light emitting diodes, IEEE Commun. Mag. 51 (2013) 148–154. doi:10.1109/MCOM.2013.6576353.

[15] C. Vega-Colado, B. Arredondo, J.C. Torres, E. López-Fraguas, R. Vergaz, D. Martín-Martín, G. Del Pozo, B. Romero, P. Apilo, X. Quintana, M. A. Geday, C. De Dios, J.M. Sánchez-Pena, An All-Organic Flexible Visible Light Communication System, Sensors. 18 (2018) 3045. doi:10.3390/s18093045.

[16] M. Liu, M.B. Johnston, H.J. Snaith, Efficient planar heterojunction perovskite solar cells by vapour deposition, Nature. 501 (2013) 395–398. doi:10.1038/nature12509.

[17] NREL Efficiency Chart. This Plot Is Courtesy of the National Renewable Energy Laboratory, Golden, CO., (n.d.). https://www.nrel.gov/pv/assets/pdfs/best-research-cell-efficiencies-190416.pdf (accessed June 7, 2019).

[18] Y. Sun, J. Peng, Y. Chen, Y. Yao, Z. Liang, Triple-cation mixed-halide perovskites: towards efficient, annealing-free and air-stable solar cells enabled by Pb(SCN)2 additive, Sci. Rep. 7 (2017). doi:10.1038/srep46193.

[19] M. Saliba, T. Matsui, J.-Y. Seo, K. Domanski, J.-P. Correa-Baena, M.K. Nazeeruddin, S.M. Zakeeruddin, W. Tress, A. Abate, A. Hagfeldt, M. Grätzel, Cesium-containing triple cation perovskite solar cells: improved stability, reproducibility and high efficiency, Energy Environ. Sci. 9 (2016) 1989–1997. doi:10.1039/C5EE03874J.

[20] W. Rehman, D.P. McMeekin, J.B. Patel, R.L. Milot, M.B. Johnston, H.J. Snaith, L.M. Herz, Photovoltaic mixed-cation lead mixed-halide perovskites: links between crystallinity, photo-stability and electronic properties, Energy Environ. Sci. 10 (2017) 361–369. doi:10.1039/C6EE03014A.

[21] L. Meng, J. You, Y. Yang, Addressing the stability issue of perovskite solar cells for commercial applications, Nat. Commun. 9 (2018) 5265. doi:10.1038/s41467-018-07255-1.

[22] G. Grancini, C. Roldán-Carmona, I. Zimmermann, E. Mosconi, X. Lee, D. Martineau, S. Narbey, F. Oswald, F. De Angelis, M. Graetzel, M.K. Nazeeruddin, One-Year stable perovskite solar cells by 2D/3D interface engineering, Nat. Commun. 8 (2017) 15684. doi:10.1038/ncomms15684.

[23] M. Gong, R. Sakidja, R. Goul, D. Ewing, M. Casper, A. Stramel, A. Elliot, J.Z. Wu, High-Performance All-Inorganic $CsPbCl_3$ Perovskite Nanocrystal Photodetectors with Superior Stability, ACS Nano. (2019). doi:10.1021/acsnano.8b07850.

[24] C. Bao, J. Yang, S. Bai, W. Xu, Z. Yan, Q. Xu, J. Liu, W. Zhang, F. Gao, High Performance and Stable All-Inorganic Metal Halide Perovskite-Based Photodetectors for Optical Communication Applications, Adv. Mater. 30 (2018) 1803422. doi:10.1002/adma.201803422.

[25] L. Dou, Y. (Micheal) Yang, J. You, Z. Hong, W.-H. Chang, G. Li, Y. Yang, Solution-processed hybrid perovskite photodetectors with high detectivity, Nat. Commun. 5 (2014) 5404. doi:10.1038/ncomms6404.

[26] C. Bao, Z. Chen, Y. Fang, H. Wei, Y. Deng, X. Xiao, L. Li, J. Huang, Low-Noise and Large-Linear-Dynamic-Range Photodetectors Based on Hybrid-Perovskite Thin-Single-Crystals, Adv. Mater. 29 (2017) 1703209. doi:10.1002/adma.201703209.

[27] X. Hu, X. Zhang, L. Liang, J. Bao, S. Li, W. Yang, Y. Xie, High-Performance Flexible Broadband Photodetector Based on Organolead Halide Perovskite, Adv. Funct. Mater. 24 (2014) 7373–7380. doi:10.1002/adfm.201402020.

[28] H. Wang, D.H. Kim, Perovskite-based photodetectors: materials and devices, Chem. Soc. Rev. 46 (2017) 5204–5236. doi:10.1039/C6CS00896H.

[29] L. Salamandra, N.Y. Nia, M. Di Natali, C. Fazolo, S. Maiello, L. La Notte, G. Susanna, A. Pizzoleo, F. Matteocci, L. Cinà, L. Mattiello, F. Brunetti, A. Di Carlo, A. Reale, Perovskite photo-detectors (PVSK-PDs) for visible light communication, Org. Electron. 69 (2019) 220–226. doi:10.1016/j.orgel.2019.03.008.

[30] M. Najafi, F. Di Giacomo, D. Zhang, S. Shanmugam, A. Senes, W. Verhees, A. Hadipour, Y. Galagan, T. Aernouts, S. Veenstra, R. Andriessen, Highly Efficient and Stable Flexible Perovskite Solar Cells with Metal Oxides Nanoparticle Charge Extraction Layers, Small Weinh. Bergstr. Ger. 14 (2018) e1702775. doi:10.1002/smll.201702775.

[31] M. Najafi, V. Zardetto, D. Zhang, D. Koushik, M.S. Dörenkämper, M. Creatore, R. Andriessen, P. Poodt, S. Veenstra, Highly Efficient and Stable Semi-Transparent p-i-n Planar Perovskite Solar Cells by Atmospheric Pressure Spatial Atomic Layer Deposited ZnO, Sol. RRL. 2 (2018) 1800147. doi:10.1002/solr.201800147.

[32] E. López-Fraguas, J.M. Sánchez-Pena, R. Vergaz, A Low-Cost LED-Based Solar Simulator, IEEE Trans. Instrum. Meas. (2019) 1–11. doi:10.1109/TIM.2019.2899513.

[33] D. Liu, M.K. Gangishetty, T.L. Kelly, Effect of CH3NH3PbI3 thickness on device efficiency in planar heterojunction perovskite solar cells, J. Mater. Chem. A. 2 (2014) 19873–19881. doi:10.1039/C4TA02637C.

[34] M. Kielar, O. Dhez, G. Pecastaings, A. Curutchet, L. Hirsch, Long-Term Stable Organic Photodetectors with Ultra Low Dark Currents for High Detectivity Applications, Sci. Rep. 6 (2016) 39201. doi:10.1038/srep39201.

[35] M. Zhang, F. Zhang, Y. Wang, L. Zhu, Y. Hu, Z. Lou, Y. Hou, F. Teng, High-Performance Photodiode-Type Photodetectors Based on Polycrystalline Formamidinium Lead Iodide Perovskite Thin Films, Sci. Rep. 8 (2018) 11157. doi:10.1038/s41598-018-29147-6.

[36] A.R. Bowring, L. Bertoluzzi, B.C. O'Regan, M.D. McGehee, Reverse Bias Behavior of Halide Perovskite Solar Cells, Adv. Energy Mater. 8 (2018) 1702365. doi:10.1002/aenm.201702365.

[37] B. Arredondo, C. de Dios, R. Vergaz, G. del Pozo, B. Romero, High-Bandwidth Organic Photodetector Analyzed by Impedance Spectroscopy, IEEE Photonics Technol. Lett. 24 (2012) 1868–1871. doi:10.1109/LPT.2012.2217488.

[38] O. Almora, I. Zarazua, E. Mas-Marza, I. Mora-Sero, J. Bisquert, G. Garcia-Belmonte, Capacitive Dark Currents, Hysteresis, and Electrode Polarization in Lead

Halide Perovskite Solar Cells, J. Phys. Chem. Lett. 6 (2015) 1645–1652. doi:10.1021/acs.jpclett.5b00480.

[39] I. Zarazua, G. Han, P.P. Boix, S. Mhaisalkar, F. Fabregat-Santiago, I. Mora-Seró, J. Bisquert, G. Garcia-Belmonte, Surface Recombination and Collection Efficiency in Perovskite Solar Cells from Impedance Analysis, J. Phys. Chem. Lett. 7 (2016) 5105–5113. doi:10.1021/acs.jpclett.6b02193.